

## A Resilient, Untethered Soft Robot

Michael T. Tolley,<sup>1,2</sup> Robert F. Shepherd,<sup>3,4</sup> Bobak Mosadegh,<sup>2,3</sup> Kevin C. Galloway,<sup>1,2</sup> Michael Wehner,<sup>1,2</sup> Michael Karpelson,<sup>1,2</sup> Robert J. Wood,<sup>1,2</sup> and George M. Whitesides<sup>2,3</sup>

### Abstract

A pneumatically powered, fully untethered mobile soft robot is described. Composites consisting of silicone elastomer, polyaramid fabric, and hollow glass microspheres were used to fabricate a sufficiently large soft robot to carry the miniature air compressors, battery, valves, and controller needed for autonomous operation. Fabrication techniques were developed to mold a 0.65-meter-long soft body with modified Pneu-Net actuators capable of operating at the elevated pressures (up to 138 kPa) required to actuate the legs of the robot and hold payloads of up to 8 kg. The soft robot is safe to interact with during operation, and its silicone body is innately resilient to a variety of adverse environmental conditions including snow, puddles of water, direct (albeit limited) exposure to flames, and the crushing force of being run over by an automobile.

### Introduction

THERE IS A NASCENT CLASS of robots—so-called soft robots—that contain no (or few) rigid internal structural elements and are loosely modeled on animals with nonrigid body parts (starfish, squid, and others).<sup>1–6</sup> Many of these soft robots are actuated pneumatically using gas transferred to them from a stationary source via a flexible tether.<sup>7–10</sup> Recent work has demonstrated robots propelled by pneumatically powered soft actuators capable of untethered operation underwater,<sup>11</sup> and on land, with rolling<sup>12</sup> and serpentine locomotion.<sup>13</sup> In addition to their soft actuators, these previous untethered soft robots also contained rigid structural components and did not locomote in gaits that required lifting their masses against gravity. The fully soft, ambulatory robots we have described previously have not been sufficiently large (presently ~15 cm in largest dimension), nor actuated at sufficiently high pressures (~0.5 atm, 7 psi, ~48 kPa) to support the size or weight of commercially available power supplies (e.g., batteries and compressed gas cylinders) and the other components (e.g., valves, air compressors, circuit boards) necessary to operate autonomously. The limitations imposed by size are one primary reason that they have been designed to function with compressed gas supplied through an external pneumatic tether. Although this tether may interfere with some tasks, it is often an advantage rather than a

disadvantage for others; for example, it enables the transfer or sampling of fluids and solids<sup>10</sup> and facilitates electronic communication and optical observation. Nonetheless, robots intended for use outside of laboratory environments should be able to operate without the constraints of a tether; this is especially true for robots intended to perform demanding tasks in challenging environments (for example, for search and rescue applications in unstable rubble).

We have developed composite soft materials, a mechanical design, and a fabrication method that enable the untethered operation of a soft robot without any rigid structural components. This robot can operate in two modes: using a battery pack (for several hours) and using a very lightweight electrical tether (for much longer periods). Though these robots are composed primarily of synthetic elastomers, we provide several demonstrations that they are capable of operating outside a forgiving laboratory environment—in a snowstorm, in puddles of water, and in direct (albeit limited) exposure to flames.

We fabricated a quadrupedal soft robot ~0.65 m in length that can be driven for 2 hours on a flat surface using a battery pack (3,200 mAh, lithium/polymer; E-flite) at speeds of >18.0 m/hr<sup>-1</sup> in a walking gait, and >2.0 m/hr<sup>-1</sup> in an undulating gait (Fig. 1). The design of the robot was based on that of a previous, tethered quadrupedal soft robot.<sup>7</sup> We modified four characteristics of the tethered robot in order to

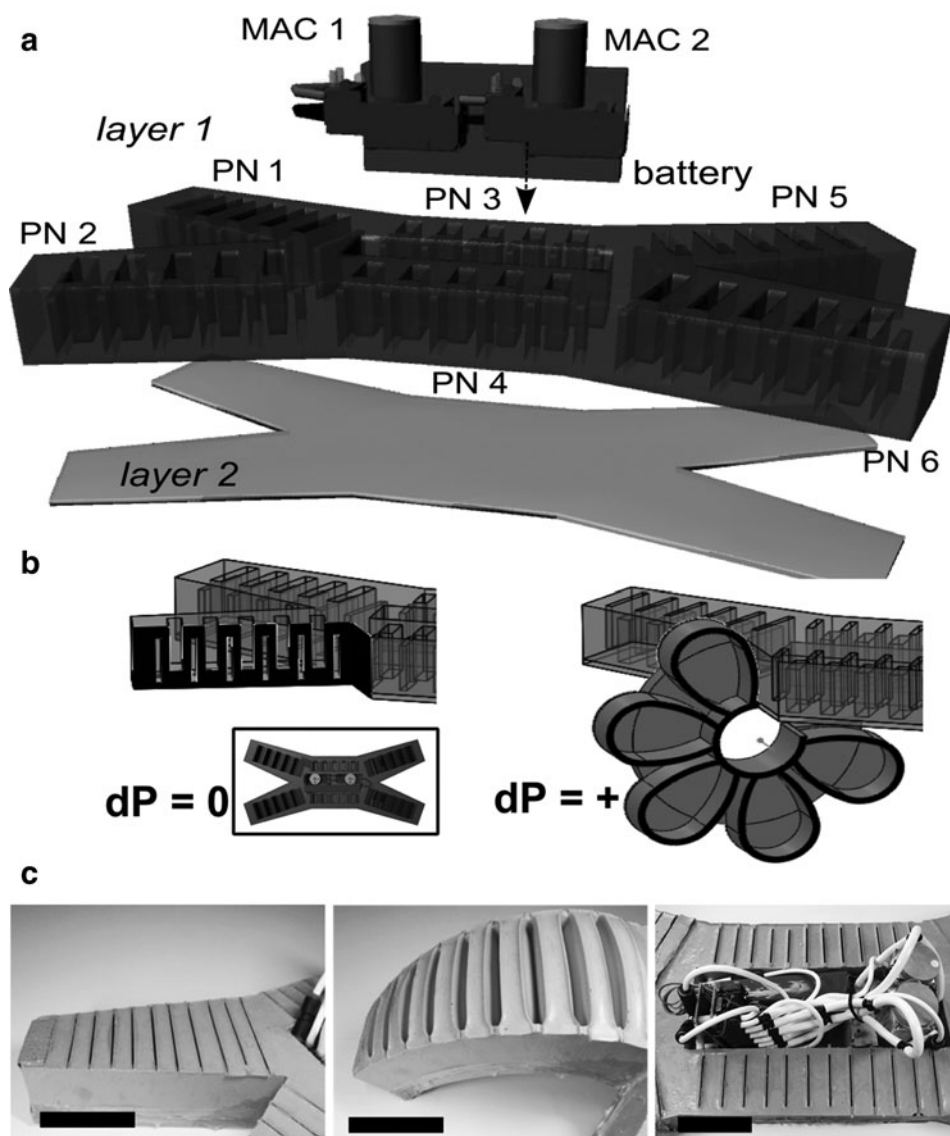
<sup>1</sup>School of Engineering and Applied Sciences, Harvard University, Cambridge, Massachusetts.

<sup>2</sup>Wyss Institute for Biologically Inspired Engineering, Harvard University, Boston, Massachusetts.

<sup>3</sup>Department of Chemistry and Chemical Biology, Harvard University, Cambridge, Massachusetts.

<sup>4</sup>School of Mechanical and Aerospace Engineering, Cornell University, Ithaca, New York.

**FIG. 1.** Pneumatic actuation of untethered quadrupedal soft robot. **(a)** Schematic representation of the components of the mini air compressor (MAC)-driven, battery powered soft robot. Layer 1 consisting of six Pneu-Nets (PN) is sealed onto layer 2. **(b)** Schematic representation of a cross-section of Pneu-Net 1 as its internal pneumatic network is pressurized. **(c)** Photographs of Pneu-Net 1 at rest (*left*) and pressurized to 16 psi (*middle*). Photograph of electronic components (mini air compressors, battery pack, relays, and circuit boards) between Pneu-Nets 3 and 4 (*right*) that drive the robot.



develop an untethered one that is resilient to a variety of environmental conditions. We (i) designed a higher strength (and lower density) composite elastomeric material for the body so that the robot could operate at higher pneumatic pressures; (ii) designed a larger body size to accommodate and support the power source; (iii) employed a modified Pneu-Net (PN) architecture<sup>14</sup> to allow more rapid and stable actuation than our previous Pneu-Net design; and (iv) incorporated an electrically powered on-board air compressor, a system of valves, and a controller for pneumatic actuation.

The robot is primarily composed of silicone rubber. This material has a glass transition temperature (depending on additives) of approximately  $-120^{\circ}\text{C}$  and thermal stability to temperatures up to  $\sim 400^{\circ}\text{C}$ .<sup>15</sup> Silicone soft robots are thus, in principle, capable of operating in environments in which temperature has a wide range. In addition, many siloxane-derived polymers are: (i) hydrophobic (i.e., water resistant) and energetically stable to corrosive, nucleo-, and electrophilic attack from many polar moieties;<sup>16</sup> (ii) resistant to ultraviolet (UV) light,<sup>15</sup> and thus stable in intense sunlight over

several decades;<sup>17</sup> and (iii) fire resistant, so capable of surviving brief, but direct, exposure to flames.<sup>18–20</sup>

### Experimental Design

The design presented here is a prototype of an untethered system that incorporates a complete set of functional elements (body, power source, control system, and sensors). The selection of these elements resulted from (and in) a set of empirical tradeoffs, and certainly does not yet represent a fully optimized set for any specific application. It was designed, instead, to give a starting point for the development of a family of untethered soft robots.

#### Material selection/design of material composites

To carry the increased load of the pneumatic pumps and control electronics, as well as a body larger than that of our prior quadrupedal robots,<sup>7</sup> we used a silicone with a higher elastic modulus ( $\sim 7.0\text{ MPa}$  or 1,015 psi; M4601, Wacker Chemicals) and similar extensibility ( $\sim 700\%$  strain to

failure) as compared to the silicone elastomer used previously (Ecoflex 0030, Smooth-On, which has an elastic modulus of  $\sim 0.11$  MPa or 16 psi<sup>7,10</sup>) (Fig. 2). This allowed us to actuate the robot with the higher internal pressures required to carry the increased load.

We reduced the weight of the body of the robot by  $\sim 40\%$  relative to scaled versions of previous designs by incorporating hollow glass spheres into the silicone (see the section Soft Composite Robot Fabrication below for experimental details). The addition of the glass spheres reduced the extensibility of the material (to  $\sim 400\%$  strain to failure), but this reduction did not compromise the operation of the robot due to the improved mechanical design of the actuators.<sup>14</sup>

#### Power source

We explored the advantages and disadvantages of using compressed gas sources and electrically operated air compressors to provide pneumatic actuation of the robot. As-

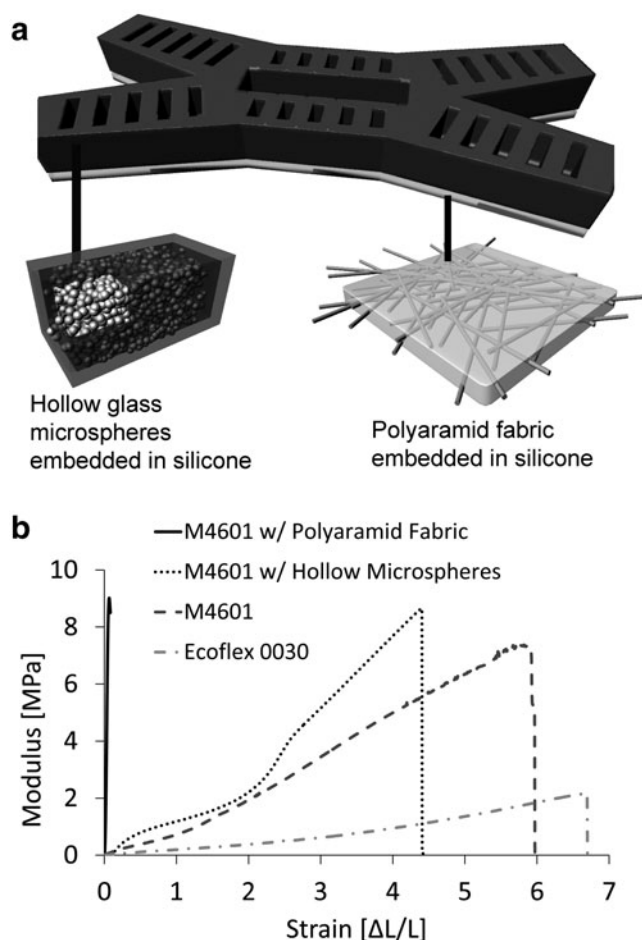


**FIG. 2.** Designing soft composites for improved material properties. (a) Two material composites are used in the soft robot. The top layer of the robot (*black*) is a blend of hollow glass spheres in silicone, and the bottom layer (*white*) is a nylon mesh impregnated with the same silicone. (b) The stress strain curves for the material comprising the top (glass bubbled M4601) and bottom layers (nylon mesh w/M4601), as well as pure M4601 and Ecoflex 0030, the material used in prior soft robots for comparison.

suming isothermal expansion at temperature  $T$  (i.e., a process slow enough for energy from the environment to heat the expanding gas), the maximum work  $w$  that can be done by  $n$  moles of gas at a working pressure,  $p_w$ , expanding to atmospheric pressure,  $p_{atm}$ , is given by Equation 1, where  $R$  is the Boltzmann constant.

$$w = nRT \ln(p_w/p_{atm}) \quad (1)$$

For a working pressure of 16 psig (214 kPa) at 20°C, a mole of compressed gas has the potential to do 1.83 kJ of work. Compressed air at the commonly available pressure of 2,900 psig (20 MPa) and 20°C has a molar volume of 8.04 kmol/m<sup>3</sup>. Pressurized carbon dioxide, however, is commonly at 850 psig (5.9 MPa) and has a molar volume of 17.8 kmol/m<sup>3</sup>. Thus, the energy density of commonly available liquid CO<sub>2</sub> is approximately 2.2 times that of gaseous compressed air. Due to this higher volumetric energy density, we used CO<sub>2</sub> (*l*) as our source for compressed gas.

Using the Hagen-Poiseuille relationship (Equation 2) between pressure difference,  $\Delta P$ ; initial flow rate of gas into a Pneu-Net volume,  $Q$ ; the gas delivery tube length,  $L$ ; and radius,  $r$ , we calculated the theoretical flow rate for compressed gas from commercially available CO<sub>2</sub> cylinders. For compressed CO<sub>2</sub> regulated to 16 psig (214 kPa) flowing through a 1 m tube with a 2.5 mm radius, the initial flow rate is 0.12 m<sup>3</sup>/s. However, this value will drop rapidly as the actuator begins to pressurize. The available volume of gas from a cylinder capable of holding 44 g of liquid CO<sub>2</sub> (a size compatible with our design) is  $\sim 10.5$  L at the working pressure.

$$\Delta P = 8\mu LQ/\pi r^4 \quad (2)$$

Mini air compressors (MACs) are relatively lightweight ( $< 0.5$  kg) diaphragm pumps driven by electrical motors. They can be operated by electrical wire from a remote location for tethered operation, or via battery in untethered operation. While tethered (using thin, light copper wires), the robot can be actuated indefinitely. Two motors powered via a 3,200 mAh lithium-polymer battery ( $\sim 0.5$  kg) can operate continuously for 1.6 hours (the motors draw  $\sim 1,000$  mA of current each). However, the mini air compressors have limited flow rates: a maximum of 11 L/min ( $1.8 \times 10^{-4}$  m<sup>3</sup>/s) unrestricted, or 2 L/min ( $3.3 \times 10^{-5}$  m<sup>3</sup>/s) at 16 psig (214 kPa). Thus, over 1.6 hours, the volume of gas at the working pressure that the compressors deliver is at least 192 L.

Though the initial flow rate of gas into a Pneu-Net provided by the MACs is lower than for compressed gas cylinders, the overall volume of gas available for actuation is much greater (192 L vs. 10.5 L). In any case, flow rates quickly become limited by back pressure in the pressurized Pneu-Net. Combined with the potential for both tethered and untethered operation, MACs were the most attractive option for our untethered soft robot. The air compressors we ultimately chose (BTC IIS, Parker Systems) were a good compromise between cost (\$297), weight (0.34 kg), size (7.5 cm length), and gas flow rates (2 L/min) at the chosen working pressure. It should be noted that a potential advantage of compressed gas is the ability to accelerate actuation with higher working pressures. However, this approach would require the development of materials and/or control systems

capable of preventing material failures caused by steady-state exposure to such elevated pressures.

### Body architecture

The body of our soft robot consists of four legs connected to a central body, each of which is actuated by a Pneu-Net, in a configuration identical to our previous, tethered quadrupedal soft robot design (Fig. 1a).<sup>7</sup> In order to increase the rate of actuation of the larger untethered robot, we used a Pneu-Net design that allows for actuation at lower pressures, and with less volumetric flow of gas into the Pneu-Nets, than our prior design (Fig. 1b).<sup>14</sup> The spine of the robot is actuated by two parallel Pnet-Nets with space between them to accommodate the power supply, control board, and two air compressors (Fig. 1c; systems diagram of compressors and valving shown in Fig. 3).

### Control system and sensors

A custom, lightweight controller board was designed to control the miniature air compressors and solenoid valves that actuate the soft robot. A microcontroller (ATmega168, Atmel Corporation) on the controller board contained an Arduino bootloader for uploading, storing, and executing programs to control the soft robot. This controller board had outputs for two mini air compressors (MACs), and six two-way valves (Ten-X, Parker Hannifin Corporation), one for each of the six PN that actuated the robot. The MACs provided a source of pressurized air at a constant rate, while the valves switched the connection of each Pneu-Net between this elevated pressure and atmospheric pressure. One MAC supplied Pneu-Nets 3 and 4, while the other MAC supplied the remaining Pneu-Nets (i.e., Pneu-Nets 1, 2, 5, and 6; see Fig. 3). To actuate one of the Pneu-Nets, the corresponding valve was opened to connect the Pneu-Net to the output of the associated MAC (as well as to any other Pneu-Net currently being actuated). While a Pneu-Net was not being actuated, it was by default being vented to the atmosphere. (A hold state was unnecessary for the patterns of pressurization and depressurization we used for actuation of the quadruped.) Using a custom-designed control board allowed us to minimize the size and mass of the control system.

Control programs were stored in the onboard memory of the controller. These programs, written and uploaded using the Arduino interface, consisted of sequences of commands to the control valves and air compressors (the MACs ran at a constant voltage). The extent of actuation of a Pneu-Net was controlled by the duration that the valve connecting it to the source of pressurized gas was opened (see the section Controls for Undulating and Walking Gaits below for details on

the control sequences used to achieve walking and ambulating gaits).

We used a lightweight camera with audio and video recording and transmission capabilities (GoPro Hero2, Woodman Labs) as a sensor when audio and visual observations were required.

## Results

### Scaling considerations

Soft lithography is a scalable molding process. We have used this method previously to fabricate a quadrupedal robot of length  $\sim 15$  cm;<sup>7</sup> the robot described here has a length of  $\sim 65$  cm (Fig. 4). With all relative dimensions kept constant, as the length,  $L$ , of the robot increases, the weight of the robot increases as  $L^3$ , and the force the actuators apply at the same  $\Delta P$  increases as  $L^2$  (pressure over the internal surface area of the Pneu-Nets). Consequently, for a particular actuating pressure, the robot will eventually become too heavy to support its own weight, much less any additional load necessary for untethered operation. Thus, for larger robots, we must reduce their density and/or increase their actuation pressure (to achieve greater actuating forces). Given the weight and size of the selected pneumatic actuation source, we estimated a required overall robot body length of  $\sim 0.65$  meters, which made our prior material choice (Ecoflex 0030) and actuation pressure (7 psi) insufficient to carry either the body of the robot or the components for untethered operation (data not shown).

### Soft composite robot fabrication

The material system we designed for the actuating layer (Fig. 1, layer 1) was low density (0.6 g/cc), high modulus (7 MPa), resilient ( $< 10\%$  loss in stored energy during cycling), tough (270 MJ/cm<sup>3</sup>), and still relatively extensible (400% strain to failure; Fig. 2b).

Because of the large size of the robot ( $\sim 0.65$  m in length), we found the use of molds assembled from pieces of laser-cut sheets of 6 mm thick acrylic to be an economical and flexible option. Using integrated alignment features, we assembled the cut acrylic pieces into a three-dimensional mold (Fig. 4b). The modular nature of these molds greatly facilitated demolding of the cast robots. We used a water-jet system to cut aluminum for the thinnest pieces of the mold, as they were most susceptible to fracture during demolding (Fig. 4c).

To fabricate the body of the soft robot, we mixed batches of the rubber composite by blending 0.15 kg of hollow glass spheres ( $\rho_{hgs} \sim 0.13$  kg/L; Microbubbles, 3M) into 1.75 kg of M4601A silicone ( $\rho_{hgs} \sim 1.2$  kg/L) using a rotational mixer and impeller blade. After mixing for 30 min, we added M4601B catalyst to the mixture at a 1:9 ratio of M4601B:M4601A by weight. After mixing for another 10 min, we poured the silicone over the laser-cut mold.

Though foams are an option to reduce the weight of the body, silicone foam prepolymers are not (to our knowledge) readily available at lab scale; it is difficult to predict the final volume of foam expansion, and available foam prepolymers (e.g., urethanes) have been difficult to bond to silicone in our lab-scale processes.

In order to prevent tears and bursting through the strain-limiting layer (Fig. 1, layer 2), we impregnated a polyaramid

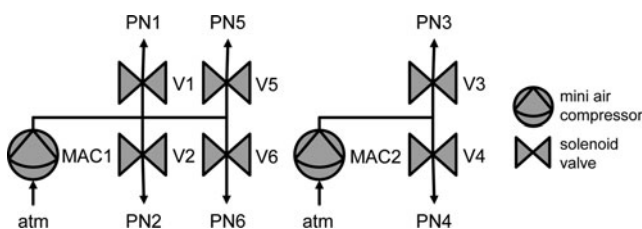


**FIG. 3.** System diagram of the configuration of mini air compressors and valves used to drive the robot in undulation or walking gaits.

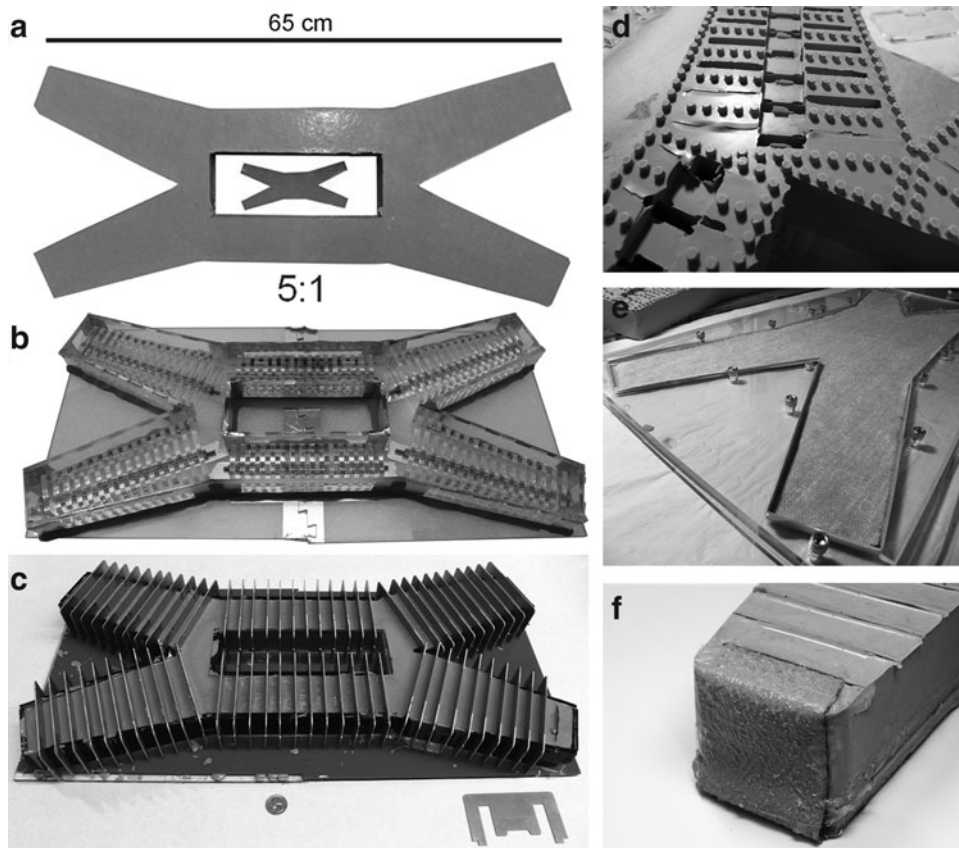


**FIG. 4.** Soft untethered robot fabrication. (a) The untethered robot design with the smaller tethered quadrupedal robot<sup>7</sup> placed on the interior for scale. The large robot is five times longer than the small one. (b) Mold used to replicate the large quadruped, composed of laser-cut acrylic pieces. (c) Layer 1 of robot cast in mold with waterjet-cut aluminum pieces inserted from the top (one aluminum piece removed from the lower right leg is shown). (d) Replicated layer 1 with molded features to increase surface area and improve bonding with layer 2. (e) Cut polyaramid fabric being impregnated with elastomer to form layer 2. (f) A patch of elastomer-impregnated polyaramid fabric added to the ends of the limbs prevents undesired expansion at these locations.

fabric with M4601 silicone in a second mold (Fig. 4e). The relative material properties of this sheet are shown in Figure 2b. We subsequently glued this composite sheet to the actuating layer using a thin ( $< 100\mu\text{m}$ ) layer of adhesive silicone sealant (Elastosil E 951; Wacker Chemical Corp.) spread between the two layers. In addition, to promote adhesion between layers, we molded pegs on the bottom of layer 1 (Fig. 4d) and complementary holes into the top of layer 2; these features increased the surface area for bonding. Similarly, we glued strips of silicone-impregnated polyaramid to the ends of the legs to limit undesired expansion at these locations (Fig. 4f).

Our choices of materials and methods of assembly allowed us to make a robot that proved resilient to many harsh conditions. As an example of the durability of the robot, we programmed the robot to walk underneath a Subaru Outback wagon (details on the actuation sequence used for walking are provided below in the section Controls for Undulating and Walking Gaits), and stop with its front legs in the path of the tires of the car. After venting all of the PNs, we drove the wagon over the soft legs of the robot at a speed of 0.34 m/s. Following a preprogrammed delay, the robot stood up and continued walking with no damage from the  $\sim 500$  kg (1,125 lbs) applied by one wheel of the vehicle (Fig. 5e–h; Supp. Video S1, available online at [www.liebertpub.com](http://www.liebertpub.com)).

#### *Internal pressure capacity, load carrying ability*

The PNs that actuate the legs (1, 2, 5, and 6) were able to sustain internal pressures of  $\sim 172$  kPa (25 psi) prior to rupturing. The two PNs that actuate the spine (3 and 4) rup-

tured at lower pressures  $\sim 152$  kPa (22 psi), probably due to a smaller area of adhesive contact for layers 1 and 2.

Starting from a flat position, a tethered version of the soft robot was able to lift a mass of 3.4 kg (7.5 lbs) when the legs and spine were pressurized to just below their maximum tolerances (139 kPa, 20 psi). Subtracting the mass of the power and control components (1.2 kg, 2.6 lbs), this represents a net payload capacity of 2.2 kg (4.9 lbs), or 44% of the total mass of the untethered robot (Fig. 6).

Once the robot is in the standing position, the lower moment arm of a central mass on the legs meant that they could carry a larger load. With an internal pneumatic pressure of 139 kPa (20 psi), the robot was able to hold a mass of 8.0 kg (17.6 lbs), or 160% of the total mass of the untethered robot.

#### *Controls for undulating and walking gaits*

**Undulating.** We implemented an undulating gait that actuated the Pneu-Nets of the robot in sequence and created an actuation wave that traveled through the body from the rear toward the front; this wave resulted in forward motion. The undulating gait consisted of repeated sequence of five states:

1. The rear leg PNs were actuated simultaneously for 7 sec (Fig. 7b).
2. The rear leg and body PNs were then actuated together for 0.5 sec.
3. The rear and forward legs, as well as the body PNs, were all actuated simultaneously for 5 sec (Fig. 7c).
4. The front legs were actuated alone for 2 sec (Fig. 7d; the differential timing in actuation between the front

**FIG. 5.** Untethered operation of the quadrupedal soft robot. (a–d) Untethered soft robot conducting indoor surveillance with the view of the onboard camera overlaid. The robot starts moving forward with a straight ambulatory gait (a). The robot switches to a turning gait to explore a passageway on the left (b, c). The robot uses its onboard camera to image a hidden laptop (d). (e–h) Untethered soft robot operating outdoors before and after being run over by a car (e). The robot depressurizes its actuators in preparation for impact (f). The car running over the elastomeric legs of the soft robot (g). The soft robot actuating and standing up after being run over by the car (h). Green dots on the figures in the upper-right corner of each frame indicate which PNs are currently actuated (pressurized); red dots indicate unactuated PNs. Color images available online at [www.liebertpub.com/soro](http://www.liebertpub.com/soro)



and back legs of approximately 5 sec biased the locomotion in the forward direction).

5. All of the PNs vented to the atmosphere for 2 sec; the MACs were also turned off for this period to facilitate venting and conserve battery power (Fig. 7e).

The actuation wave of the undulating gait resulted in forward motion at a velocity of  $\sim 2.0 \text{ m/hr}^{-1}$  (Supp Video S2).

**Walking.** To achieve a walking gait, we used a second program with a gait cycle consisting of two strides, each of which consisted of four states:

1. Beginning with all legs in contact with the ground (to prevent the robot from slipping backward), we caused the rear leg to actuate for 4 sec, resulting in a stance position (Fig. 7h).

2. The actuated rear leg, as well as the front leg on the opposite side of the body, were then actuated simultaneously for 4 sec to transfer both the pressurized air and the weight of the robot from the rear leg to the front one (reusing pressurized air during this transfer step increased the efficiency of the robot.)
3. The robot then thrust itself forward by both, depressurizing the rear leg (allowing the stored elastic energy to straighten the rear leg), while continuing to pressurize the front leg to pull the robot forward over the course of 4 sec (Fig. 7i).
4. We then briefly connected both the pressurized front leg and the rear leg on the same side of the robot to high pressure (for 0.5 sec) to begin deflation of the front leg and inflation of the rear leg for the next actuation cycle (Fig. 7g).

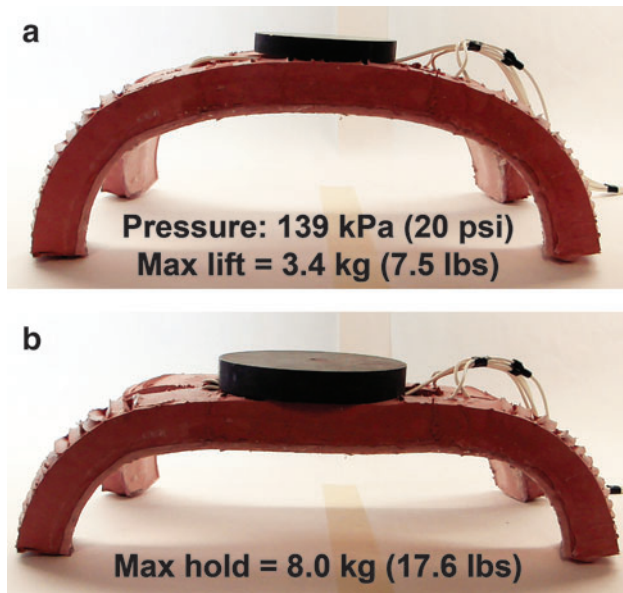


**FIG. 6.** Maximum lift and hold tests. **(a)** Starting from a flat position, a tethered version of the soft robot was able to lift a mass of 3.4 kg (7.5 lbs) when actuated with a pneumatic pressure of 139 kPa (20 psi). **(b)** Starting from an actuated position with an internal pneumatic pressure of 139 kPa (20 psi), the robot was able to hold 8.0 kg (17.6 lbs). Color images available online at [www.liebertpub.com/soro](http://www.liebertpub.com/soro)

Repeating the above four steps on alternating sides of the body resulted in our walking gait. The timing of the actuation for all four legs over a complete walking gait cycle is shown in Figure 8. The center PNs (3 and 4) were inflated throughout the gait to arch the back of the robot. The walking gait

allowed the robot to travel at a velocity of  $\sim 18.0 \text{ m/hr}^{-1}$  (Supp. Video S2).

We analyzed the motion of the robot during the walking gait using motion tracking software (ProAnalyst, Xcitex Inc.; Fig. 9). By tracking markers drawn onto the surface of the robot (Fig. 9a), we calculated the change in the heading (yaw) of the robot over a few representative gait cycles (Fig. 9b). The heading of the robot deviated sinusoidally during each gait cycle, with maximum deviations of  $\pm 8$  deg. Similarly, tracking the horizon on video filmed from a camera attached to the robot gave an estimate of the transverse inclination (roll) of the robot (Fig. 9c and d). During the walking gait, the robot inclined periodically to a maximum of  $\pm 45$  deg. Note that because of changes in the robot over time, the open-loop actuation timings had to be adjusted, resulting in slightly different gait cycle periods.

**Turning.** We caused the robot to turn by halving the duration of actuations during one stride of the walking gait. For example, in Figure 5b–d, PNs 1 and 6 were actuated for half the duration of PNs 2 and 5. The result was a left turn with a radius of approximately 150 cm (a little more than two body lengths). Figure 10 shows the position and heading of the robot after 13 turning gait cycles for 3 successive runs (recorded from experiment videos). Over all three runs (39 cycles), the robot rotated an average of 5.1 deg per gait cycle, with a standard deviation of  $\pm 0.99^\circ$ .

*Remote audio and video sensing: Ambulating into a small passageway*

By strapping a forward-facing camera onto the body of the robot, we were able to perform remote audio and video

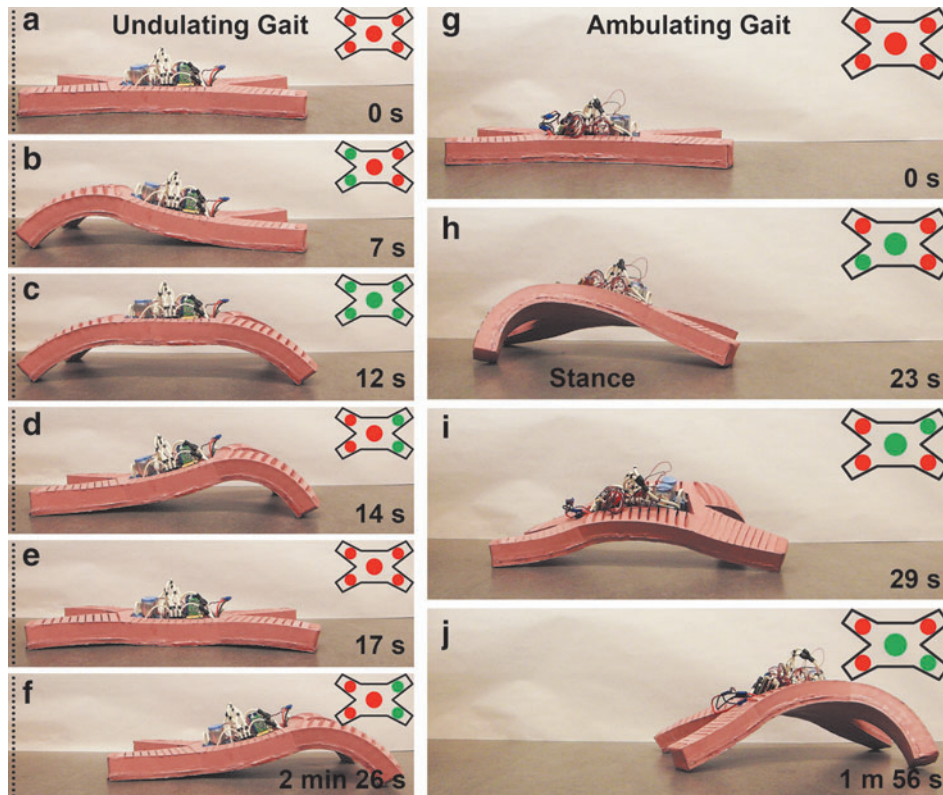
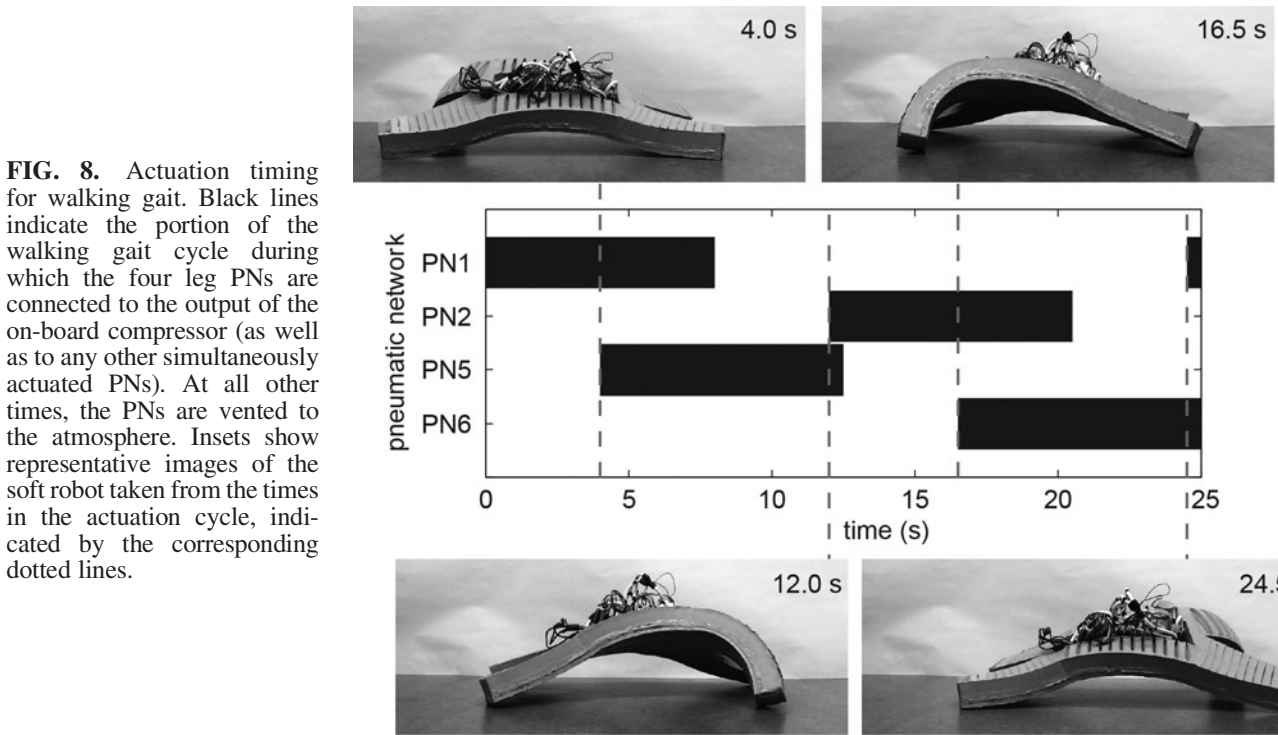


**FIG. 7.** Frames from movies of the untethered soft robot executing undulating and ambulating gaits. **(a–f)** Undulating gait: The pneumatic channels are inflated sequentially from the rear of the robot toward the front, resulting in forward motion. Dotted lines mark the starting position for reference. **(g–j)** Ambulating gait: Starting from rest **(g)**, a rear leg is actuated **(h)**, the opposite front leg is then actuated to shift the weight forward **(i)**. This sequence is repeated on alternating sides, resulting in a straight ambulatory gait **(j)**. Green dots on the figures in the upper-right corner of each frame indicate which PNs are currently actuated (pressurized); red dots indicate unactuated PNs. The time elapsed since the start of the gait is indicated on each frame. Color images available online at [www.liebertpub.com/soro](http://www.liebertpub.com/soro)

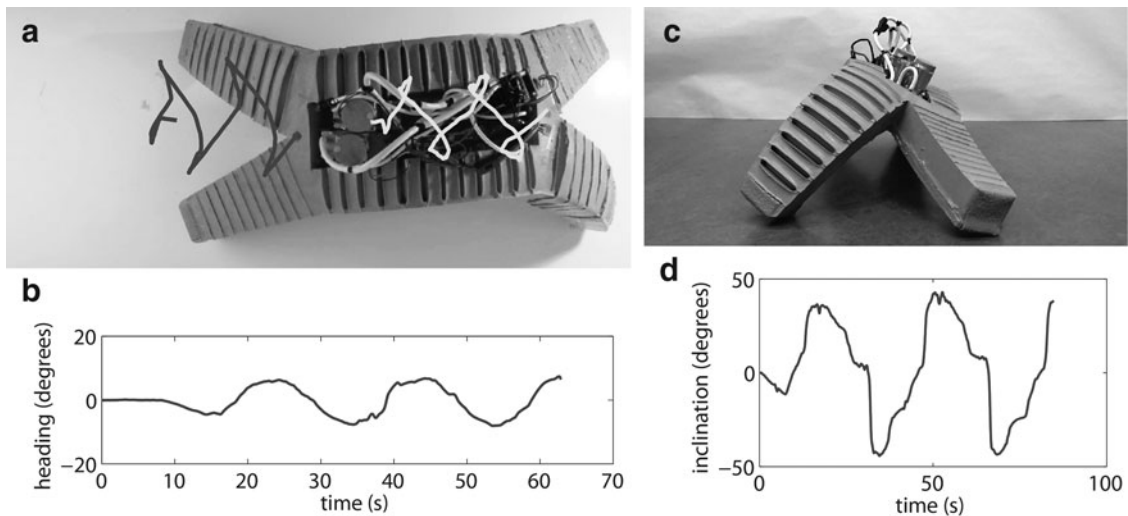


sensing (of a laboratory, Fig. 5a–d; Supp. Video S3). For this demonstration, the information from the camera was recorded and stored on the onboard controller; the recorded audio and video were retrieved at the end of the trial.

#### Resilience to harsh environments

The material, and monolithic design, of our untethered soft robot enable it to withstand a variety of harsh environmental conditions against which traditional robots must be carefully protected (Fig. 11 and Supp. Video S1).

Our robot successfully executed its walking gait outside during a snowstorm (Winter Storm Nemo) with an average temperature of  $-9^{\circ}\text{C}$  ( $15^{\circ}\text{F}$ ), and average wind speed of 40 km/h (25 mph, Figure 11a). Because of the low glass transition temperature of the robot's body material (approximately  $-120^{\circ}\text{C}$ ),<sup>17</sup> as well as the lack of sliding parts (e.g., bearings) to be contaminated, the robot ambulated normally in the snow and cold weather. Because the elastic modulus of silicone rubber is relatively constant in the range of  $-20^{\circ}\text{C}$  to  $300^{\circ}\text{C}$  ( $-4^{\circ}\text{F}$  to  $572^{\circ}\text{F}$ ),<sup>21</sup> pneumatic actuation was not impeded by the cold temperatures (although we did not develop



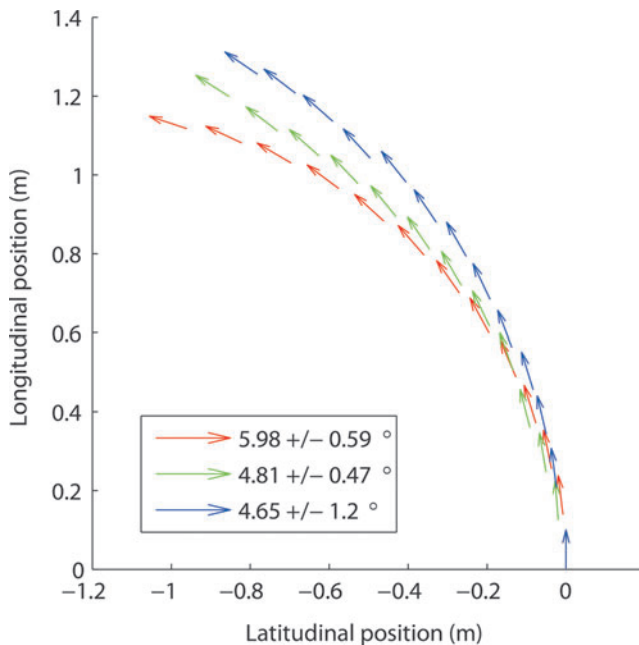


**FIG. 10.** Turning paths for 13 gait cycles of 3 successive runs. Locations and heading of the robot were recorded at the same point in the gait cycle from experimental videos. Color images available online at [www.liebertpub.com/soro](http://www.liebertpub.com/soro)

specialized feet for travelling through snow). The robot also walked successfully in wet, slushy conditions at temperatures near 0°C or 32°F (Figure 5e-h; Video S1).

We commanded the robot to walk down a ramp into a plastic tray filled with 5 cm (2 in) of water (Figure 11b). The body of the robot is hydrophobic and inherently sealed against water (and is also resistant to acids).<sup>10,16</sup> It suffered no damage walking through water.

We manually controlled the ambulation of a tethered version of the soft robot across a metal grating through two flames produced through the combustion of methane gas in Bunsen burners (Figure 11c). The longest duration of direct flame exposure an element of the robot sustained was 20 seconds. Despite the exposure to extremely high temperatures ( $\sim 3,000$  K),<sup>18</sup> the robot suffered only superficial damage due to the resistance of the silicone rubber to fire and high temperatures. Silicone rubbers are known to produce fire-retarding silica-ash layers when exposed to flames, and can be exposed to direct flames for  $\sim 50$  seconds before any permanent damage occurs.<sup>19,20</sup>

## Discussion

We designed a 0.65-m-long soft robot without any rigid structural components that can carry its own weight, all the components necessary for up to 2 h of untethered operation, plus an additional payload (e.g., surveillance equipment), across smooth terrain.

This resilient soft robot was enabled by the careful selection of materials and design of soft material composites. We used a silicone (M4601) that was tougher than that used previously (Ecoflex 0030) to support larger loads (the body of the robot, plus components for untethered operation). We added glass hollow spheres to the silicone to reduce its weight. Although the glass hollow spheres reduced the ex-

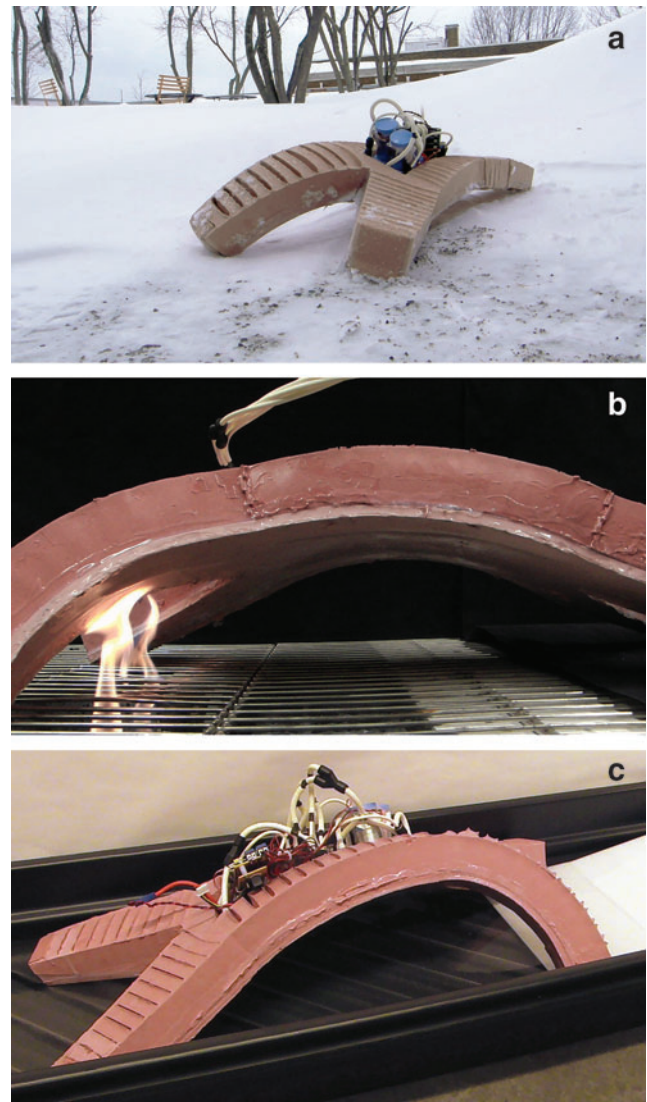


**FIG. 11.** Resilience of the untethered soft robot to harsh conditions. (a–c) Images from experiments of the soft robot operating untethered in a variety of harsh conditions, including a snow storm (a), a fire (b), and water (c). Color images available online at [www.liebertpub.com/soro](http://www.liebertpub.com/soro)

tensibility of the material, they did not reduce the toughness of the material (the integral of the stress-strain curve). Simultaneously, the new design of the Pneu-Net architecture<sup>14</sup> allows the use of the slightly less extensible composite with no loss in functionality.

We demonstrated the capabilities and surprising resilience of this soft robot experimentally. We developed a turning gait and showed multigait capabilities in this larger soft robot; we performed untethered video reconnaissance, suitable for search and rescue missions; and we tested the robot in a range of harsh environmental conditions.

## Conclusions

Silicone robots inherit the strength of silicone rubbers including being impervious to water, good acid/base stability, and resistance to damage from blunt impacts or applied pressures. They are also safer in direct contact with humans. In

TABLE 1. MATERIALS COSTS FOR THE SOFT ROBOT PROTOTYPE

<i>Component</i>	<i>Count</i>	<i>Unit cost</i>	<i>Extended cost</i>
<b>Body materials</b>			
Elastosil M4601 silicone rubber	3.5 kg	\$21/kg	\$74
Hollow glass spheres	0.3 kg	\$150/kg (\$75/gal)	\$45
Polyaramid fabric	12" × 40"	\$16	\$16
Elastosil E951 silicone sealant	1 tube	\$19	\$19
<b>Power and control components</b>			
Mini air compressors	2	\$297	\$594
Valves	6	\$43	\$258
Battery pack	1	\$45	\$45
Custom controller board	1	\$40	\$40
Tubing and fittings	-	-	\$20
<b>Total</b>			<b>\$1111</b>

addition, monolithic molded mechanisms (such as the body of the robot presented here) are relatively less expensive (see Table 1 for a full cost breakdown of our soft robot prototype) and less prone to failure than their assembled counterparts due to the absence of sliding parts (e.g., bearings), and reduced assembly interfaces and associated fasteners/adhesives. Pneumatically actuated soft robots do, however, also have disadvantages with respect to hard robots, including sensitivity to large holes or tears by sharp objects, decreased precision and ability to track prescribed motions, and relatively slower actuation (although rapid actuation—100 ms for actuation over a complete range of motion—is possible with practical designs).<sup>14</sup> The balance of these advantages and disadvantages determine the suitability of pneumatically actuated soft robots for any particular application.

The design of the soft robot presented here has the additional advantages over previous hard and soft robots of autonomy of power, good operation time between battery charges, the capabilities of audio and video sensing, and the capacity to carry larger payloads for a desired task.

One weakness of the design presented here is the sensitivity of the exposed, rigid components at the center of the robot (compressors, valves, controller, batteries) to the conditions that typically challenge rigid robots (blunt impacts, applied pressures, and harsh environmental conditions). It may be possible to alleviate this weakness by distributing the rigid components over the body of the robot and encasing them in the soft body material. Another, more technically challenging option is to replace the rigid components with soft counterparts. This approach, however, requires significant breakthroughs in the development of soft electronics, batteries, and pumps. One promising option is to use passive soft components wherever possible (e.g., passive addressable valves).<sup>22</sup>

Another challenge with the design presented here is the slow locomotion speed of the robot, which is limited by the flow rate of air into the pneumatic actuators. This flow rate is, in turn, limited by the output pressure of the onboard compressors, as well as the flow restrictions caused by the onboard valves and tubing. Larger compressors, valves, and tubing all lead to a larger mass that must be carried by the body. Nonetheless, it may be possible to optimize these components to improve the overall speed of the robot. Alternative modes of pressurization (i.e., combustion) can be used to increase actuation speeds.<sup>18</sup>

Furthermore, the nonoptimized feet and single degree-of-freedom legs of the robot limit it to operation on flat surfaces

and at relatively low speeds. Optimization of the design of the legs and feet of the robot for locomotion would likely increase its speed and overall mobility. The approach we have taken here is to alter the pneumatic network design to minimize unproductive expansion of the elastomer.<sup>14</sup> It may be possible to further improve actuation speeds and mobility with additional fibers or fabric to limit unwanted expansion and the use of actuators with multiple degrees of freedom per leg.<sup>10,23–26</sup> Modification of the coefficient of friction between the soft robot and the surface upon which it is walking could also improve the speed of locomotion.<sup>27</sup>

A final limitation of the current design is the requirement of preprogrammed control sequences. However, the addition of off-the-shelf bidirectional communication hardware (e.g., Xbee Wireless RF modules) would allow remote operation with live video feedback. The further development of feedback control strategies based on the available audio and/or video sensors, or additional touch, smell, or other sensors that can be integrated into the soft robot design,<sup>28–31</sup> would allow for completely autonomous operation.

### Acknowledgments

The development of the design, materials, and controls system was supported by DARPA under award number W911NF-11-1-0094, NSF under award number DMR-0820484, and the Wyss Institute for Biologically Inspired Engineering. The analysis and testing of power sources was supported by the Department of Energy under award number DE-FG02-00ER45852. Any opinions, findings, and conclusions or recommendations expressed in this material are those of the authors and do not necessarily reflect the views of the National Science Foundation. The authors would also like to acknowledge Dr. Yigit Menguc for helpful discussions and his assistance with the use of motion tracking software.

### Author Disclosure Statement

No competing financial interests exist.

### References

1. Trivedi D, Rahn CD, Kier WM, Walker ID. Soft robotics: Biological inspiration, state of the art, and future research. *Applied Bionics and Biomechanics* 2008; 5(3):99–117.
2. Cho K-J, Koh J-S, Kim S, Chu W-S, Hong Y, Ahn S-H. Review of manufacturing processes for soft biomimetic

- robots. *International Journal of Precision Engineering and Manufacturing* 2009; 10(3):171–181.
3. Pfeifer R, Lungarella M, Iida F. The challenges ahead for bio-inspired soft robotics. *Commun ACM* 2012; 55(11):76–87.
  4. Kim S, Laschi C, Trimmer B. Soft robotics: a bioinspired evolution in robotics. *Trends Biotechnol* 2013; 31(5):287–294.
  5. Lipson H. Challenges and opportunities for design, simulation, and fabrication of soft robots. *Soft Robotics* 2013; 1(P):21–27.
  6. Majidi C. Soft robotics: A perspective current trends and prospects for the future. *Soft Robotics* 2013; 1(P):5–11.
  7. Shepherd RF, Ilievski F, Choi W, Morin SA, Stokes AA, Mazzeo AD, Chen X, Wang M, Whitesides GM. Multigait soft robot. *Proceedings of the National Academy of Sciences* 2011; 108(51):20400–20403.
  8. Ilievski F, Mazzeo AD, Shepherd RF, Chen X, Whitesides GM. Soft robotics for chemists. *Angewandte Chemie* 2011; 123(8):1930–1935.
  9. Stokes AA, Shepherd RF, Morin SA, Ilievski F, Whitesides GM. A hybrid combining hard and soft robots. *Soft Robotics* 2013; 1(P):70–74.
  10. Martinez RV, Branch JL, Fish CR, Jin L, Shepherd RF, Nunes R, Suo Z, Whitesides GM. Robotic tentacles with three-dimensional mobility based on flexible elastomers. *Advanced Materials* 2013; 25(2):205–212.
  11. Marchese AD, Onal CD, Rus D. Autonomous soft robotic fish capable of escape maneuvers using fluidic elastomer actuators. *Soft Robotics* 2014; 1(1):75–87.
  12. Onal CD, Chen X, Whitesides GM, Rus D. Soft mobile robots with on-board chemical pressure generation. *In International Symposium on Robotics Research* 2011, pp. 1–16.
  13. Onal CD, Rus D. Autonomous undulatory serpentine locomotion utilizing body dynamics of a fluidic soft robot. *Bioinspir Biomim* 2013; 8(2):026003.
  14. Mosadegh B, Polygerinos P, Keplinger C, Wennstedt S, Shepherd RF, Gupta U, Shim J, Bertoldi K, Walsh CJ, Whitesides GM. Pneumatic networks for soft robotics that actuate rapidly. *Advanced Functional Materials* 2013; 24(15):2163–2170.
  15. Zheng P, McCarthy TJ. Rediscovering silicones: Molecularly smooth, low surface energy, unfilled, uv/vis-transparent, extremely cross-linked, thermally stable, hard, elastic pdms. *Langmuir* 2010; 26(24):18585–18590.
  16. Chang C-L, Lee HS-J, Chen C-K. Nucleophilic cleavage of crosslinked polysiloxanes to cyclic siloxane monomers: Mild catalysis by a designed polar solvent system. *Journal of Polymer Research* 2005; 12(6):433–438.
  17. Oldfield D, Symes T. Long term natural ageing of silicone elastomers. *Polymer Testing* 1996; 15(2):115–128.
  18. Shepherd RF, Stokes AA, Freake J, Barber J, Snyder PW, Mazzeo AD, Cademartiri L, Morin SA, Whitesides GM. Using explosions to power a soft robot. *Angewandte Chemie* 2013; 125(10):2964–2968.
  19. Hsieh F-Y. Shielding effects of silica-ash layer on the combustion of silicones and their possible applications on the fire retardancy of organic polymers. *Fire and Materials* 1998; 22(2):69–76.
  20. Hamdani S, Longuet C, Perrin D, Lopez-cuesta J-M, Ganachaud F. Flame retardancy of silicone-based materials. *Polymer Degradation and Stability* 2009; 94(4):465–495.
  21. Characteristic properties of silicone rubber compounds, Shin-Etsu Chemical Co., Tokyo, Japan, Mar 2005. Available at [www.silicone.jp/e/catalog/pdf/rubber\\_e.pdf](http://www.silicone.jp/e/catalog/pdf/rubber_e.pdf) (accessed Aug. 18, 2014).
  22. Napp N, Araki B, Tolley MT, Nagpal R, Wood RJ. Simple passive valves for addressable pneumatic actuation. *In Robotics and Automation (ICRA), 2014 IEEE International Conference on* 2014.
  23. Suzumori K, Iikura S, Tanaka H. Development of flexible microactuator and its applications to robotic mechanisms. *In Proceedings, 1991 IEEE International Conference on Robotics and Automation*; 1622–1627.
  24. Bishop-Moser J, Krishnan G, Kim C, Kota S. Design of soft robotic actuators using fluid-filled fiber-reinforced elastomeric enclosures in parallel combinations. *In 2012 IEEE/RSJ International Conference on Intelligent Robots and Systems (IROS)*; 4264–4269.
  25. Galloway KC, Polygerinos P, Walsh CJ, Wood RJ. Mechanically programmable bend radius for fiber-reinforced soft actuators. *In 2013 16th International Conference on Advanced Robotics (ICAR)*; 1–6.
  26. Marchese AD, Komorowski K, Onal CD, Rus D. Design and control of a soft and continuously deformable 2d robotic manipulation system. *In Proceedings of IEEE International Conference on Robotics and Automation* 2014.
  27. Majidi C, Shepherd RF, Kramer RK, Whitesides GM, Wood RJ. Influence of surface traction on soft robot undulation. *The International Journal of Robotics Research* 2013; 32(13):1577–1584.
  28. Majidi C, Kramer R, Wood RJ. A non-differential elastomer curvature sensor for softer-than-skin electronics. *Smart Materials and Structures* 2011; 20(10):105017.
  29. Park Y-L, Chen B-R, Wood RJ. Design and fabrication of soft artificial skin using embedded microchannels and liquid conductors. *Sensors Journal, IEEE* 2012; 12(8):2711–2718.
  30. Vogt DM, Park Y-L, Wood RJ. Design and characterization of a soft multi-axis force sensor using embedded microfluidic channels. *Sensors Journal, IEEE*, 2013; 13(10):4056–4064.
  31. Menguc Y, Park Y-L, Martinez-Villalpando E, Aubin P, Zisook M, Stirling L, Wood RJ, Walsh CJ. Soft wearable motion sensing suit for lower limb biomechanics measurements. *In 2013 IEEE International Conference on Robotics and Automation (ICRA)*; 5309–5316.

Address correspondence to:

George M. Whitesides  
Department of Chemistry and Chemical Biology  
Harvard University  
12 Oxford Street  
Cambridge, MA 02138

E-mail: [gwhitesides@gmgroup.harvard.edu](mailto:gwhitesides@gmgroup.harvard.edu)